JOURNAL OF TISSUE ENGINEERING AND REGENERATIVE MEDICINE
J Tissue Eng Regen Med 2008; **2**: 455–462.
Published online 13 October 2008 in Wiley InterScience (www.interscience.wiley.com) **DOI:** 10.1002/term.117

RESEARCH ARTICLE

Titanium foam-bioactive nanofiber hybrids for bone regeneration

Timothy D. Sargeant[1], Scott M. Oppenheimer[1], David C. Dunand[1] and Samuel I. Stupp[2]*
[1]*Department of Materials Science and Engineering, Northwestern University, Evanston, IL 60208-3108, USA*
[2]*Department of Materials Science and Engineering, Department of Chemistry, Feinberg School of Medicine, Northwestern University, Evanston, IL 60208-3108, USA*

Abstract

We have reported previously a method to introduce bioactive nanofiber networks through self-assembly into the pores of titanium alloy foams for bone repair. In this study we evaluate the *in vitro* colonization by mouse pre-osteoblastic cells of these metal–peptide amphiphile hybrids containing phosphoserine residues and the RGDS epitope. The aim was to determine the effect of varying the RGDS epitope concentration within a given range, and confirm the ability for cells to infiltrate and survive within the nanofiber-filled interconnected porosity of the hybrid material. We performed proliferation (DNA content) and differentiation assays (alkaline phosphatase and osteopontin expression) as well as SEM and confocal microscopy to evaluate cell colonization of the hybrids. At the RGDS epitope concentrations used in the nanofiber networks, all samples demonstrated significant cell migration into the hybrids, proliferation, and differentiation into osteoblastic lineage. Copyright © 2008 John Wiley & Sons, Ltd.

Received 4 April 2008; Revised 11 July 2008; Accepted 14 July 2008

Keywords regenerative medicine; tissue engineering; self-assembly; bone; Ti–6Al–4V; foam; peptide amphiphile; RGDS

1. Introduction

Titanium and its alloys remain the materials of choice for many orthopaedic and dental implants, due to the combination of excellent mechanical properties and biocompatibility. Compared with other biomedical alloys, such as stainless steels and cobalt–chrome (CoCr) alloys, titanium alloys have lower moduli, enhanced corrosion resistance and good fatigue strength (Long and Rack, 1998). Additionally, their surface oxide layer provides good biocompatibility *in vivo* (Singh and Dahotre, 2007). In recent years there has been significant work on the development of porous metals for implants to provide fixation via bone ingrowth, while also reducing the material's elastic modulus to minimize bone resorption due to stress shielding (Kienapfel *et al*., 1999; Dunand, 2004; Greiner *et al*., 2005). However, these metals lack any specific bioactivity for bone tissue formation, which has led to extensive research on titanium surface treatments and coatings (Morra, 2006).

Early efforts on the modification of titanium for bioactivity were directed towards the modification of surface topography (Martin *et al*., 1995; Boyan *et al*., 2001), and later to coatings of various types of calcium phosphates (Campbell *et al*., 1996; Toworfe *et al*., 2006) and apatites (Ong and Chan, 2000; Spoerke and Stupp, 2003). More recently, efforts have been directed towards surface modification with peptides and other biological molecules (Garcia, 2005). Rather than just coating metals, we believe an interesting approach would be to *fill* the open, interconnected porosity of porous metals with a bioactive self-assembling scaffold obtained by introducing a liquid into the voids of the metallic implant. We first reported the development of self-assembling biomaterials with biodegradable structures (Hwang *et al*., 2002; Klok *et al*., 2002a, 2002b) and more recently others containing bioactive structures (Hartgerink *et al*., 2001; Beniash *et al*., 2005). The bioactive materials have been used to develop a Ti–6Al–4V foam filled with a self-assembled,

*Correspondence to: Samuel I. Stupp, Department of Materials Science and Engineering, Department of Chemistry, Feinberg School of Medicine, Northwestern University, Evanston, IL 60208-3108, USA. E-mail: s-stupp@northwestern.edu

peptide amphiphile (PA) nanofiber matrix that we refer to as a PA–Ti hybrid (Sargeant *et al.*, 2008).

The approach of filling metal pores with bioactive nanofibers has several advantages. First, an organic scaffold is provided through which cells can be encouraged to migrate, lay down their own extracellular matrix and then remodel. Second, the molecular nature of PA nanofibers offers the possibility of tailoring bioactivity of the matrix by controlling the orientation and density of bioactive peptide epitopes (Storrie *et al.*, 2007). It is also possible in these systems to co-assemble peptide amphiphiles, either to combine epitopes or to dilute epitopes (Niece *et al.*, 2003; Behanna *et al.*, 2005). We recently showed that the concentration of RGDS epitopes on nanofibers controls cellular adhesion, and optimal adhesion was observed when the epitope is mixed with a non-bioactive PA (Storrie *et al.*, 2007). The influence of RGDS epitope presentation by nanofibers on proliferation and differentiation had not been previously examined with these PA nanofibers within a three-dimensional context. We study here the effect of RGDS epitope presentation on nanofibers within pores of PA–Ti hybrids on the proliferation, colonization and differentiation of pre-osteoblastic mouse calvarial cells *in vitro*.

2. Materials and methods

All chemical reagents, unless otherwise noted, were purchased from Sigma-Aldrich (St. Louis, MO, USA). Solvents were purchased from Fisher Scientific (Hanover Park, IL, USA). Amino acids were purchased from EMD Biosciences (San Diego, CA, USA). Cellular medium components were purchased from Invitrogen (Carlsbad, CA, USA) and other cell culture supplies from VWR (West Chester, PA, USA). MC3T3–E1 pre-osteoblastic cells were generously provided by Professor Lonnie Shea (Northwestern University, Evanston, IL, USA), and pEGFP-N1 vector was generously provided by Dr Earl Cheng (Children's Memorial Hospital, Chicago, IL, USA).

2.1. PA–Ti hybrid preparation

PA–Ti hybrids were prepared as previously reported (Sargeant *et al.*, 2008). Peptide amphiphiles (PA) were synthesized using solid-phase peptide synthesis methods previously described (Guler *et al.*, 2005, 2006) and characterized using MALDI–TOF and analytical HPLC. Ti–6Al–4V foams were created by procedures established previously for superplastic foaming (Davis *et al.*, 2001; Murray and Dunand, 2003, 2004, 2006; Murray *et al.*, 2003). The foamed Ti–6Al–4V billet was cut into $1 \times 4 \times 4\ mm^3$ samples using a diamond saw with oil lubrication, and then ultrasonically cleaned with dichloromethane, acetone and water for 15 min each. To remove metal smearing over the external pores from cutting, the samples were exposed to an aqueous solution of 0.25% HF and 2.5% HNO_3 for 45 min. After repassivation with 40% HNO_3 for 30 min, the samples were repeatedly rinsed in ultrapure water and dried in a desiccator.

PA–Ti hybrids were then prepared with different ratios of a phosphoserine-containing PA, C16AAALLLEES(P)G [S(P) PA] and an Arg–Gly–Asp–Ser-containing PA, C16AAALLLKKRGDS (RGDS PA). The PAs both contain a C_{16} tail to drive self-assembly, which is attached to a β-sheet inducing peptide sequence (AAALLL). The two glutamic acid and lysine residues, respectively, provide charge for solubility and help to promote mixing of the PAs. The S(P) residue is used to promote the formation of calcium phosphate mineral, while the RGDS sequence is used to promote cellular adhesion. Three ratios were used: 0.5 mol% RGDS PA with 99.5 mol% S(P) PA; 5 mol% RGDS PA with 95 mol% S(P) PA; and 15 mol% RGDS PA with 85 mol% S(P) PA. Lyophilized PA powders were solubilized at 10 mM in ultrapure water, adjusted to pH 7, and UV-sterilized for 25 min. S(P) PA and RGDS PA were mixed at the appropriate ratios and ultra-sonicated for 20 min at 50 °C to promote mixing. Meanwhile, Ti foams were autoclave-sterilized and pre-wetted via graded soakings starting with 100% ethanol and ending with 100% ultrapure water. Pre-wetted Ti foam samples were then placed in 75 µl of the appropriate mixed PA solutions, and agitated on a plate shaker at low speed for 30 min to promote PA infiltration. The PA solutions containing the Ti foams were then gelled with the addition of 5 µl of 1 M $CaCl_2$ each, resulting in a final $CaCl_2$ concentration of 62.5 mM. Following gelation, samples were annealed by incubation at 37 °C and 5% CO_2 for 1.5 h.

2.2. Cell culture

Mouse calvarial pre-osteoblastic (MC3T3–E1) cells were cultured under standard tissue culture conditions at 37 °C and 5% CO_2 in minimum essential medium α (MEMα) supplemented with 10% fetal bovine serum (FBS), 100 U/ml penicillin and streptomycin, 10 mM β-glycerophosphate and 50 µg/mL ascorbic acid, hereafter referred to as 'growth medium'. To enable fluorescence confocal imaging, MC3T3–E1 cells were transfected with a vector for green fluorescent protein (GFP). This was achieved by plating cells at >90% confluency in antibiotic-free growth medium without serum, adding 1 µg pEGFP–N1 vector and 2.3 µl Lipofectamine™ 2000 transfection reagent (Invitrogen), mixing gently and incubating for 24 h at 37 °C. The cells were then passaged and cultured in growth medium for 1 day, followed by medium exchange with a 'selection medium' consisting of penicillin/streptomycin-free growth medium with the addition of 600 µg/ml Geneticin® selective antibiotic (Invitrogen). Cells were cultured in the selection medium for 14 days, followed by culturing in a 'maintenance medium', consisting of penicillin/streptomycin-free growth medium with the addition of 300 µg/ml Geneticin® selective antibiotic.

DOI: 10.1002/term

Cells were then sorted by flow cytometry to obtain a homogeneous population for cell experiments, hereafter termed 'GFP–MC3T3–E1' cells. All experiments were performed using GFP–MC3T3–E1 cells in maintenance medium.

The PA–Ti hybrids were cultured in a rotating bioreactor as described by Speorke *et al*. (2005). This method of culture provides more uniform cell seeding and culture conditions without the effects of gravity compared to traditional 2D well-plate culture. Samples with 1 mm holes drilled in the middle were placed on steel skewers with Teflon spacers and a Teflon plug at the end, and inserted into a pre-conditioned rotating 110 ml STLV bioreactor culture vessel (Synthecon, Houston, TX, USA) at 37 °C and 5% CO_2. To begin culture, 10^7 GFP–MC3T3–E1 cells were added in 110 ml maintenance medium for 16 h to allow cells to adhere to the samples. The medium was then replaced with fresh maintenance medium (designated as time 0) and again every 3 days. Samples were harvested at days 1, 7, 14, 21 and 28, with the exception of samples for alkaline phosphatase (ALP) and osteocalcin (OC) analysis, which were harvested at days 1, 6, 13, 20 and 27 and cultured for 1 more day in a 96-well plate under the same conditions.

Cells were also cultured in PA gels *without* Ti foams to determine any effect of S(P) on proliferation by mixing the S(P) PA with a non-bioactive serine-containing PA (S PA). This PA was analogous is design to the S(P) PA, with the single letter amino acid sequence C_{16}AAALLLEESG (S PA). By mixing this S PA with the S(P) PA, the only variable was the concentration of the S(P) residue. For comparison with the PA–Ti hybrids, PA gels were made with 0.5 mol% S PA and 99.5 mol% S(P) PA, 5 mol% S PA and 95 mol% S(P) PA, and 15 mol% S PA and 85 mol% S(P) PA. This allowed us to single out the effect, if any, of S(P) on cell proliferation. Cells were encapsulated in 10 mM PA gels by mixing a cell suspension in maintenance medium 1 : 1 with 20 mM PA solution, triggering self-assembly of the PA. The cells were then cultured in well plates at 37 °C and 5% CO_2 for 14 days.

2.3. Biological analysis

For cell quantification, PA–Ti hybrid samples and PA gel samples were extracted and frozen in liquid nitrogen, lyophilized and digested in a papain solution (Allen *et al*., 1999). Samples were incubated in 0.125 mg/ml papain activated with 1.76 mg/ml cysteine in phosphate buffer with EDTA (0.1 M Na_2HPO_4, 0.01 M Na_2EDTA, pH adjusted with 1 N NaOH) for 16 h at 60 °C. Samples were then assayed for dsDNA content using a Quant-iT PicoGreen dsDNA Assay Kit (Molecular Probes) according to the manufacturer's protocol. A 5 µl aliquot of digestion solution was incubated with 95 µl 1× TE and 100 µl PicoGreen Working Reagent for 5 min, and fluorescence was measured on a Gemini EM fluorescence/chemiluminescence plate reader with excitation/emission of 480/520 nm. A standard curve was prepared, using a known number of cells, and used to determine the sample values.

PA–Ti hybrid samples for SEM and confocal microscopy were extracted and pre-fixed with 1% gluteraldehyde in MEMα on ice for 1 h. Samples were rinsed in PBS for 20 min and fixed in 2% formaldehyde, 2% gluteraldehyde in 0.1 M cacodylate buffer for 3 h at room temperature and then overnight at 4 °C. Samples were then rinsed in cacodylate buffer for 20 min and dehydrated using a graded series of increasing ethanol concentrations. SEM samples were critical-point dried, coated with 3 nm Au–Pd, and imaged, using a Hitachi S-4500 with a cold field emission electron gun, at 3 kV with a current of 20 mA. A secondary electron detector was used for high-resolution imaging. Alternatively, samples for confocal microscopy were embedded in EmBed-812/DER 73 (Electron Microscopy Sciences) according to the manufacturer's protocol. Samples were soaked in propylene oxide for 20 min, followed by 50 : 50 solution of EMbed-812/DER 73 and propylene oxide overnight, and then straight EMbed-812/DER 73, with several fresh exchanges. The resin was then cured for 24 h each at 40 °C, 60 °C and 70 °C. Embedded samples were sectioned using a diamond saw and mounted on glass slides. Imaging was performed on a Leica Confocal Laser Scanning System inverted microscope, using an argon laser and driven with Leica Confocal Software.

PA–Ti hybrids for alkaline phosphatase (ALP) and osteocalcin (OC) assays were removed from the bioreactor and placed into a 96-well plate with 75 µl fresh maintenance medium for 24 h at 37 °C and 5% CO_2. The medium was collected from each sample and frozen at −20 °C for 1 day, and then at −70 °C until the assay was performed. ALP was assayed using an ALP Liquicolor kit (No. 2900) from Stanbio, according to the protocol, and data were normalized relative to a maintenance medium control. OC was assayed using a Mouse Osteocalcin ELISA kit (BT-470; Biomedical Technologies) according to the protocol.

2.4. Statistical analysis

Multivariate analysis was performed using JMP 6 software to determine significance values (α) and power values (P). For individual comparisons, t-test with unknown variance was used to determine two-tailed p values. Significance was set at $\alpha = 0.05$. Statistics for biological analysis are shown using 95% confidence error bars.

3. Results and discussion

In order to evaluate the ability of cells to grow on the PA–Ti hybrid and into the pores filled with PA matrix, a cell quantification assay was performed on three different PA–Ti hybrids cultured in a rotating bioreactor for up to 28 days. The hybrids contained either 0.5 mol% RGDS PA with 99.5 mol% S(P) PA; 5 mol% RGDS PA with

DOI: 10.1002/term

95 mol% S(P) PA; or 15 mol% RGDS PA with 85 mol% S(P) PA, and will hereafter be referred to as 0.5% RGDS, 5% RGDS, and 15% RGDS hybrids, respectively. With all PA mixtures containing high concentrations of the S(P) residue, all hybrids were capable of mineralizing, keeping this effect constant throughout the experiments. The results shown in Figure 1 indicate a significant effect of time on cell proliferation for all sample types ($\alpha = 0.05$, $p = 1.00$). There is not a significant effect ($\alpha = 0.05$) on cell number between the sample types at any time point with the exception of day 14, when 15% RGDS PA–Ti hybrids had significantly higher number of cells than the other two hybrid types. Furthermore, there appears to be a maximum viable cell density that is reached by day 21 for all sample types. This plateau is maintained at day 28, with a mean cell density of 3.6×10^5 cells/sample. A similar plateau was observed for MC3T3–E1 proliferation on bare titanium foam scaffolds by St-Pierre *et al.* (2005). In that system, cell proliferation ceased after 9 days and the cell density was maintained until day 17. For the PA–Ti hybrids, the data indicate that, in the range of RGDS epitope density studied, there is not a correlation between the average concentration of RGDS epitopes and the number of cells that initially attach or the final cell density. However, higher concentrations of RGDS epitopes appear to shorten the time necessary to reach maximum cell density. This observed response could be important in the context of clinical bone regeneration as well as *ex vivo* cell seeding of scaffolds prior to implantation. This result is also interesting in the context of previous studies on the role of RGD ligands on cell adhesion and motility. Several studies have shown that in controlled experiments with serum-free medium, the concentration and clustering of RGD-containing ligands led to controllable cellular adhesion (Maheshwari *et al.*, 2000; Li *et al.*, 2006; Storrie *et al.*, 2007). However, in normal culture conditions containing serum, adsorbed proteins can mask this effect, and could be applicable to the hybrids studied here. However, during the exponential growth stage observed between days 7 and 14, there is a significant increase in proliferation for the 15% RGDS hybrids. By day 21, all samples are statistically similar, displaying a typical sigmoidal growth behaviour and reaching a plateau (St-Pierre *et al.*, 2005). Therefore, one could suggest that when exponential growth is occurring the bioactive nanostructures are able to supplement media proteins to effectively signal the larger cell population. For smaller cell populations, media proteins may be sufficient to sustain initial cell adhesion. Final cell density is possibly regulated by other mechanisms, such as contact inhibition. Therefore, in the clinical context, it may be possible to utilize the bioactive matrix to increase the rate of regeneration.

To confirm that the observed effect of increased proliferation was due to the variation in RGDS concentration and not to the variation in S(P) concentration, a proliferation assay without the RGDS epitopes was performed. This was accomplished using the same S(P) concentrations, but instead mixing with a non-bioactive PA at 0.5%, 5% and 15% as before. The results of the cell quantification assay are shown in Figure 2. The results demonstrate that the S(P) epitope does not affect the proliferation of the cells during the period of exponential growth. This confirms that the RGDS epitopes are responsible for the increased proliferation observed for the PA–Ti hybrids. Consequently, the 15% RGDS PA–Ti hybrid was used in all of the experiments described below.

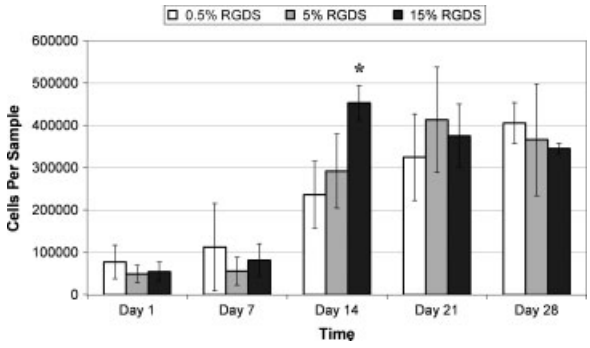

Figure 1. Graph depicting the number of cells as a function of days cultured on PA–Ti hybrids in a rotating bioreactor ($n = 8$). There is an overall statistical effect of time on cell number ($\alpha = 0.05$, $P = 1.00$). At particular time points, significant differences are indicated by asterisks ($\alpha = 0.05$). There is not a significant difference in the initial cell seeding at day 0 or in the final cell density at days 21 and 28. There appears to be a critical cell density that is reached between 2 and 3 weeks, with a mean value of 3.6×10^5 cells at day 28. There is a significant increase in cells on the 15% RGDS hybrids at day 14 compared to 0.5% and 5% RGDS hybrids

To better understand the way in which these PA–Ti hybrids are colonized by the pre-osteoblastic cells, samples were imaged by SEM and in cross-section by confocal microscopy. PA–Ti hybrids were imaged by SEM at each time-point, and were observed to be similar for each sample group at a given time. Figure 3 shows representative SEM images of 15% RGDS PA–Ti hybrids at day 1, with cells observed to be adherent and spread

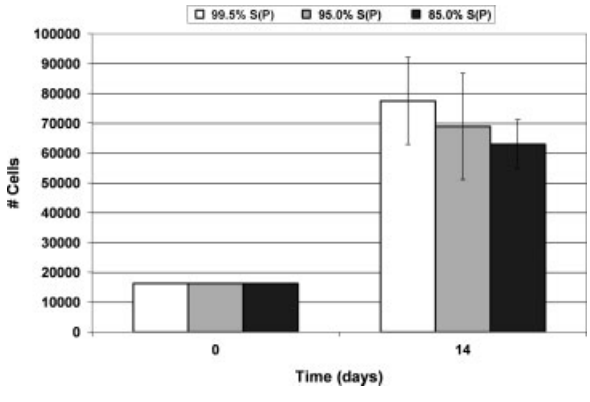

Figure 2. Number of MC3T3–E1 cells as a function of days cultured in S(P) and S PA gels. The ratios of S(P):S is the same as the ratio of S(P):RGDS used in the experiment shown in Figure 1. There is no significant difference amongst the different sample types at day 0 or day 14 using $\alpha = 0.05$. The data indicates that the increase in proliferation observed in Figure 1 is not a function of the S(P) PA

DOI: 10.1002/term

on the surface of the hybrid. There is a clear interaction between the cells and the underlying PA nanofibers, with the cells extending filopodia to bind the matrix. SEM images of 15% RGDS PA–Ti hybrids at days 1, 7 and 21 demonstrate the surface colonization of the cells (Figure 4). At day 1, much of the hybrid is still visible, with cells adherent to portions of the exterior at low confluency. By day 7, less of the hybrid exterior is visible, with cells having proliferated to cover a significant amount of the exterior and beginning to form cell–cell contacts. By day 21, the underlying hybrid is completely covered with a confluent cell layer, and the hybrid is only visible in areas where the cell layer has cracked from the processing of the samples for SEM imaging. Cellular interaction with the PA matrix and cellular migration into the hybrids by day 7 is illustrated in Figure 5. In Figure 5A, a cell is seen stretching across a gap and extending filopodia to adhere to PA nanofibers, indicated by arrows. In Figure 5B, cells are seen lining the rim of a pore, and cells are observed to be migrating into the interior (arrow) of the hybrid by pulling on the PA matrix and Ti substrate. This clearly demonstrates the preference of the cells for the PA matrix, including their ability to adhere specifically to the PA nanofibres and migrate into the hybrid.

Confocal images of cross-sectioned samples were also taken to determine the extent of migration and proliferation into the core of the hybrids. Representative images at days 1, 7 and 28 are shown of a 15% RGDS PA–Ti hybrid in Figure 6. The GFP-transfected MC3T3–E1 pre-osteoblastic cells fluoresce green, reflection from the top surface of the Ti foam appears white, and the PA nanofiber matrix is not visible. By day 1 the cells are seen to be

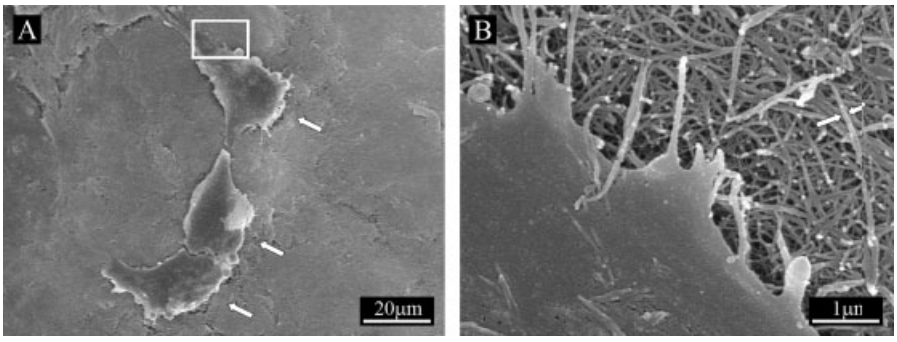

Figure 3. SEM images of MC3T3–E1 pre-osteoblastic cells cultured for 1 day on 15% RGDS PA–Ti hybrids in a rotating bioreactor. (A) Cells, indicated by arrows, spread on the exterior of the hybrid. (B) High magnification of the boxed area in (A), revealing the filopodia of the cell reaching out to the underlying PA nanofibres

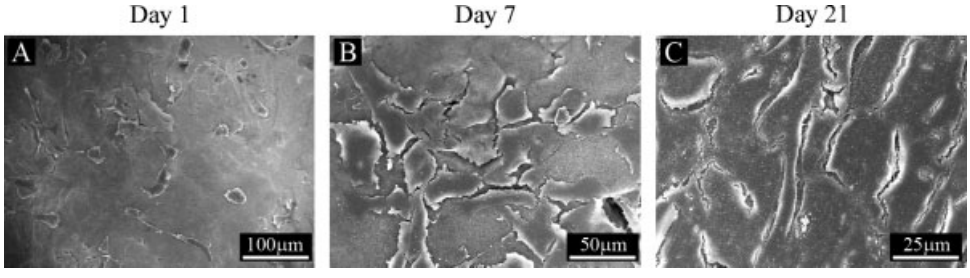

Figure 4. SEM images of 15% RGDS PA–Ti hybrids cultured for 1 (A), 7 (B) and 21 (C) days. After 1 day of culture, cells adhere and begin to spread on the exterior of the hybrids (A). By day 7, the cells have covered a significant amount of the hybrid exterior (B). By day 21, the exterior of the implant is completely covered with cells (C)

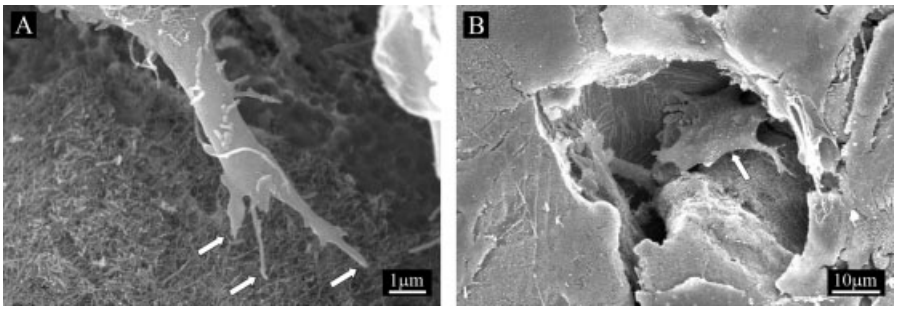

Figure 5. SEM images of MC3T3–E1 pre-osteoblastic cells cultured for 7 days on 15% RGDS PA–Ti hybrids in a rotating bioreactor. (A) A cell that is stretched across a gap and adhering to the PA matrix (indicated by arrows). (B) A cell that is migrating into the PA matrix-filled porosity of the PA–Ti hybrid (arrow)

DOI: 10.1002/term

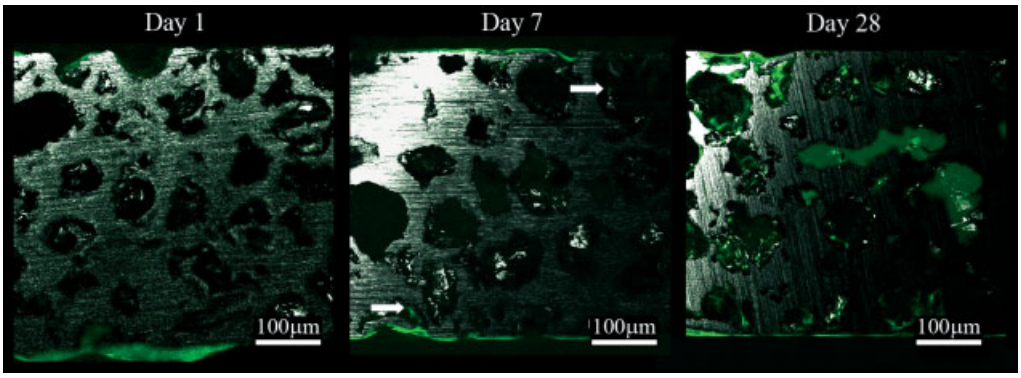

Figure 6. Confocal fluorescent images of cross-sectioned 15% RGDS PA–Ti hybrids at days 1, 7 and 28, showing GFP-transfected MC3T3–E1 pre-osteoblastic cellular ingrowth and proliferation. The cells are shown in green, with the top surface of the metal reflecting white, and the PA matrix not visible. At day 1 cells adhere to the exterior of the implant and proceed to migrate and proliferate into the core of the PA–Ti hybrid up to 28 days. At 28 days cells are observed both adjacent to the pore wall and in the PA matrix in the centre of the pores

adherent and spread on portions of the exterior of the implant, and by day 7 the cells have covered most of the exterior surface, in agreement with the SEM images. Furthermore, the confocal image at day 7 additionally shows that cells have begun to migrate into the hybrid (indicated with arrows), confirming the observation indicated by the SEM image in Figure 5B. By day 28, cells have migrated throughout the entire thickness of the hybrid via the PA matrix-filled interconnected porosity. Cells are shown both lining the rims of some pores and in the middle of the PA matrix of others. This indicates that the hybrids show an excellent capacity to facilitate ingrowth and maintain cellular viability in the core of the hybrid. Furthermore, the transfection of the cells is not expected to be absolutely complete and may diminish slightly with time, so the fluorescence observed gives a lower bound of the potential cells that are actually present. Also, deposited ECM matrix, mineral or remodelled PA matrix will not fluoresce, so areas that appear absent of cells may indeed be filled by one of these components. This implies that the dimensions of the pores and interconnects are sufficient for nutrient diffusion, even when the exterior of the hybrid is fully covered in a confluent cell layer. The 165 μm average pore size of these PA–Ti hybrids (Sargeant *et al.*, 2008) also corresponds with the generally well-accepted ideal pore size of approximately 150–400 μm for bone ingrowth and vascularization (Bobyn *et al.*, 1980; Ayers *et al.*, 1999; Wen *et al.*, 2001).

To assess the progression of differentiation of the pre-osteoblastic cells, two markers for the osteoblastic lineage were assayed: alkaline phosphatase (ALP) for early pre-osteoblastic and osteoblastic stages of differentiation, and osteocalcin (OC) for later osteoblastic and osteocytic stages of differentiation (Aubin *et al.*, 1995). As the pre-osteoblasts differentiate into osteoblasts and then osteocytes, we would expect a decrease in ALP production and an increase in OC production. ALP and OC were assayed for at each time point and normalized to the cell number from the DNA quantification assay. ALP production showed a statistically significant decrease with time for each of the hybrid types ($\alpha = 0.05$, $P = 0.9719$)

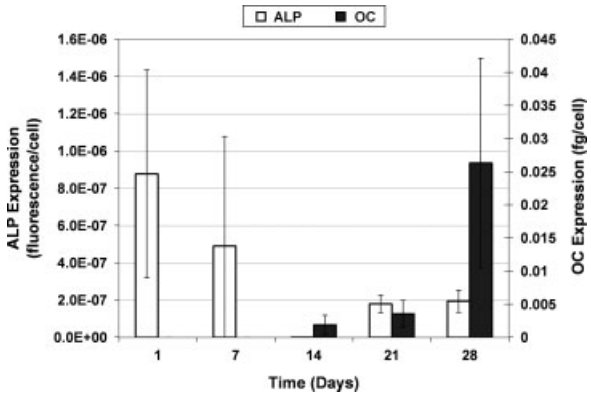

Figure 7. Alkaline phosphatase (ALP) and osteocalcin (OC) expression as a function of days cultured in a bioreactor ($n = 4$). The results are shown after background subtraction. There is a significant effect of time on both ALP production ($\alpha = 0.05$, $P = 0.9719$) and OC production ($\alpha = 0.05$, $P = 1.00$)

(Figure 7). In contrast, OC production shows a statistically significant increase as a function of time in culture ($\alpha = 0.05$, $P = 1.00$). Combining the ALP and OC data, there is clear evidence for differentiation along the osteoblastic lineage with time for the PA–Ti hybrids. Based on the compilation of differentiation data by Aubin *et al.* (1995), these MC3T3–E1 cells have matured to osteoblasts by 14 days and may have begun to mature to osteocytes by day 21 or 28. Traditionally, osteoblast differentiation follows three stages: proliferation, matrix synthesis and maturation, and then mineralization (Lian and Stein, 1992; Liu *et al.*, 1994; Aubin *et al.*, 1995). This was observed by St. Pierre *et al.* (2005), who studied MC3T3–E1 colonization of bare titanium foam and measured an increase in ALP production when the proliferation reached a plateau. However, they observed a concurrent increase in OC at the same time as ALP, and both decreased shortly thereafter. This does not correspond with the linear progression of pre-osteoblastic cells (Lian and Stein, 1992; Liu *et al.*, 1994; Aubin *et al.*, 1995), and was attributed by St-Pierre *et al.* to the cells responding to different mechanisms that may be

DOI: 10.1002/term

influenced by TGFβ interaction with the titanium scaffold. In the work presented here, the ALP expression from cells in the PA–Ti hybrids is elevated during the first week while the proliferation rate is low. It is postulated that as the cells initially adhere and begin to migrate into the PA–Ti hybrid, the cell density is low and proliferation is minimal, allowing the cells to secrete ALP, the marker expected at their pre-osteoblastic stage of differentiation. Once the cells start to grow into the implant and the proliferation rate increases during week 2, the ALP expression level decreases. Indeed, we observed cells migrating into the PA–Ti hybrids by day 7, as shown in Figures 5B and 6. After 14 days, the samples approach their cell density plateau and OC expression increases, signalling their maturation into osteoblasts and the onset of mineralization of their ECM. Our data therefore suggest that PA–Ti hybrids facilitate the differentiation of pre-osteoblastic cells along the osteoblastic lineage.

4. Conclusions

We have developed metal-bioactive nanofiber hybrid materials using peptide amphiphile self-assembly within the pores of titanium foam. We observed the effective attachment, spreading and migration of pre-osteoblasts into the interior of these hybrids. A plateau density of cells is reached faster in hybrid samples containing nanofibers with 15% molar density of RGDS relative to other samples. Based on expression of alkaline phosphatase and osteocalcin in these bioactive hybrids, we also conclude that pre-osteoblastic cells are able to mature along the osteoblastic lineage by day 14, when a cell density plateau is reached. The modification of porous metals with bioactive nanostructures is a possible strategy to accelerate bone regeneration at tissue interfaces with implants.

Acknowledgements

The authors gratefully acknowledge funding support from the National Science Foundation, under Award No. DMR-0505772, and the National Institutes of Health, under Award No. 5R01DE015920. Electron microscopy was performed in the Electron Probe Instrumentation Center (EPIC) facility of the NUANCE Center at Northwestern University, and is supported by NSF-NSEC, NSF-MRSEC, the Keck Foundation, the State of Illinois, and Northwestern University. Confocal microscopy was performed in the Biological Imaging Facility (BIF) at Northwestern University. Cell work was performed in the Institute for BioNanotechnology in Medicine (IBNAM) at Northwestern University. We thank Mr Ben Myers for his technical help with experiments at EPIC and Dr William Russin and Ms Ramona Walsh for their technical help with experiments at BIF.

References

Allen R, Eisenberg S, Gray M. 1999; *Tissue Engineering Methods and Protocols*. Humana Press: Totowa, NJ, USA.

Aubin JE, Liu F, Malaval L, *et al*. 1995; Osteoblast and chondroblast differentiation. *Bone* **17**: S77–S83.

Ayers RA, Simske SJ, Bateman TA, *et al*. 1999; Effect of nitinol implant porosity on cranial bone ingrowth and apposition after 6 weeks. *J Biomed Mater Res* **45**: 42–47.

Behanna HA, Donners JJJM, Gordon AC, *et al*. 2005; Coassembly of amphiphiles with opposite peptide polarities into nanofibres. *J Am Chem Soc* **127**: 1193–1200.

Beniash E, Hartgerink JD, Storrie H, *et al*. 2005; Self-assembling peptide amphiphile nanofibre matrices for cell entrapment. *Acta Biomater* **1**: 387–397.

Bobyn JD, Pilliar RM, Cameron HU, *et al*. 1980; The optimum pore-size for the fixation of porous-surfaced metal implants by the ingrowth of bone. *Clin Orthop Relat Res* 263–270.

Boyan BD, Lohmann CH, Dean DD, *et al*. 2001; Mechanisms involved in osteoblast response to implant surface morphology. *Annu Rev Mater Res* **31**: 357–371.

Campbell AA, Fryxell GE, Linehan JC, *et al*. 1996; Surface-induced mineralization: a new method for producing calcium phosphate coatings. *J Biomed Mater Res* **32**: 111–118.

Davis NG, Teisen J, Schuh C, *et al*. 2001; Solid-state foaming of titanium by superplastic expansion of argon-filled pores. *J Mater Res* **16**: 1508–1519.

Dunand DC. 2004; Processing of titanium foams. *Adv Eng Mater* **6**: 369–376.

Garcia AJ. 2005; Get a grip: integrins in cell–biomaterial interactions. *Biomaterials* **26**: 7525–7529.

Greiner C, Oppenheimer SM, Dunand DC. 2005; High strength, low stiffness, porous NiTi with superelastic properties. *Acta Biomater* **1**: 705–716.

Guler MO, Hsu L, Soukasene S, *et al*. 2006; Presentation of RGDS epitopes on self-assembled nanofibres of branched peptide amphiphiles. *Biomacromolecules* **7**: 1855–1863.

Guler MO, Soukasene S, Hulvat JF, *et al*. 2005; Presentation and recognition of biotin on nanofibres formed by branched peptide amphiphiles. *Nano Lett* **5**: 249–252.

Hartgerink JD, Beniash E, Stupp SI. 2001; Self-assembly and mineralization of peptide–amphiphile nanofibres. *Science* **294**: 1684–1688.

Hwang JJ, Iyer SN, Li L-S, *et al*. 2002; Self-assembling biomaterials: liquid crystal phases of cholesteryl oligo(L-lactic acid) and their interactions with cells. *Proc Natl Acad Sci USA* **99**: 9662–9667.

Kienapfel H, Sprey C, Wilke A, *et al*. 1999; Implant fixation by bone ingrowth *J Arthroplasty* **14**: 355–368.

Klok HA, Hwang JJ, Hartgerink JD, *et al*. 2002a; Self-assembling Biomaterials: L-lysine-dendron-substituted cholesteryl-(L-lactic acid)*n*. *Macromolecules* **35**: 6101–6111.

Klok HA, Hwang JJ, Iyer SN, *et al*. 2002b; Cholesteryl-(L-lactic acid)*n* building blocks for self-assembling biomaterials. *Macromolecules* **35**: 746–759.

Li J, Yun H, Gong YD, *et al*. 2006; Investigation of MC3T3–E1 cell behavior on the surface of GRGDS-coupled chitosan. *Biomacromolecules* **7**: 1112–1123.

Lian JB, Stein GS. 1992; Concepts of osteoblast growth and differentiation – basis for modulation of bone cell development and tissue formation. *Crit Rev Oral Biol Med* **3**: 269–305.

Liu F, Malaval L, Gupta AK, *et al*. 1994; Simultaneous detection of multiple bone-related messenger-RNAs and protein expression during osteoblast differentiation – polymerase chain reaction and immunocytochemical studies at the single-cell level. *Dev Biol* **166**: 220–234.

Long M, Rack HJ. 1998; Titanium alloys in total joint replacement – a materials science perspective. *Biomaterials* **19**: 1621–1639.

Maheshwari G, Brown G, Lauffenburger DA, *et al*. 2000; Cell adhesion and motility depend on nanoscale RGD clustering *J Cell Sci* **113**: 1677–1686.

Martin JY, Schwartz Z, Hummert TW, *et al*. 1995; Effect of titanium surface-roughness on proliferation, differentiation, and protein synthesis of human osteoblast-like cells (Mg63). *J Biomed Mater Res* **29**: 389–401.

Morra M. 2006; Biochemical modification of titanium surfaces: peptides and ECM proteins. *Eur Cell Mater* **12**: 1–15.

Murray NGD, Dunand DC. 2003; Microstructure evolution during solid-state foaming of titanium. *Composites Sci Technol* **63**: 2311–2316.

Murray NGD, Dunand DC. 2004; Effect of thermal history on the superplastic expansion of argon-filled pores in titanium: Part I. Kinetics and microstructure. *Acta Mater* **52**: 2269–2278.

Murray NGD, Dunand DC. 2006; Effect of initial preform porosity on solid-state foaming of titanium. *J Mater Res* **21**: 1175–1188.
Murray NGD, Schuh CA, Dunand DC. 2003; Solid-state foaming of titanium by hydrogen-induced internal-stress superplasticity. *Scr Mater* **49**: 879–883.
Niece KL, Hartgerink JD, Donners JJJM, *et al*. 2003; Self-assembly combining two bioactive peptide-amphiphile molecules into nanofibres by electrostatic attraction. *J Am Chem Soc* **125**: 7146–7147.
Ong JL, Chan DC. 2000; Hydroxyapatite and their use as coatings in dental implants: a review. *Crit Rev Biomed Eng* **28**: 667–707.
Sargeant TD, Guler MO, Oppenheimer SM, *et al*. 2008; Hybrid bone implants: self-assembly of peptide amphiphile nanofibres within porous titanium. *Biomaterials* **29**: 161–171.
Singh R, Dahotre NB. 2007; Corrosion degradation and prevention by surface modification of biometallic materials. *J Mater Sci Mater Med* **18**: 725–751.
Spoerke ED, Murray NG, Li H, *et al*. 2005; A bioactive titanium foam scaffold for bone repair. *Acta Biomater* **1**: 523–533.
Spoerke ED, Stupp SI. 2003; Colonization of organoapatite-titanium mesh by preosteoblastic cells. *J Biomed Mater Res A* **67**: 960–969.
St-Pierre JP, Gauthier M, Lefebvre LP, *et al*. 2005; Three-dimensional growth of differentiating MC3T3–E1 pre-osteoblasts on porous titanium scaffolds. *Biomaterials* **26**: 7319–7328.
Storrie H, Guler MO, Abu-Amara SN, *et al*. 2007; Supramolecular crafting of cell adhesion. *Biomaterials* **28**: 4608–4618.
Toworfe GK, Composto RJ, Shapiro IM, *et al*. 2006; Nucleation and growth of calcium phosphate on amine-, carboxyl- and hydroxyl-silane self-assembled monolayers. *Biomaterials* **27**: 631–642.
Wen CE, Mabuchi M, Yamada Y, *et al*. 2001; Processing of biocompatible porous Ti and Mg. *Scr Mater* **45**: 1147–1153.

DOI: 10.1002/term